A study on Co doped SnO_2 loaded corn cob activated carbon for the photocatalytic degradation of methylene blue dye

Ragupathy S (ragupathymsc@gmail.com)
ERK arts and Science college https://orcid.org/0000-0001-5314-0646
Ramamoorthy M
Periyar University

Research Article

Keywords: SnO2 NPs, Co doping, Activated carbon, Photocatalytic activity, Methylene Blue

Posted Date: February 23rd, 2021

DOI: https://doi.org/10.21203/rs.3.rs-168313/v1

Abstract

SnO_2 with different Co^{2+} doping concentrations (0.050, 0.075 and 0.10 M), and Co (0.075 M): SnO_2/corn cob activated carbon (Co: SnO_2/CCAC) were prepared, and are labelled CS1, CS2, CS3 and CS2/CCAC respectively. The CS2/CCAC showed that the particle size is reduced (16.29 nm) with Co^{2+} doping and CCAC loading. Moreover, CS2/CCAC indicate that the decreased PL intensity and its lower value (2.156 Ω) of impedance from EIS results and increased separation of the photogenerated e^-/h^+ pairs. Thus, the result showed that CS2/CCAC possesses improved photocatalytic efficiency (95.38 %) as compared to other samples. The photocatalytic mechanism of CS2/CCAC also is discussed.

1. Introduction

In recent years, organic and inorganic contamination due to population and industrial growth has been increased. Among these, organic contamination is a critical environmental problem in the world one. They are, organic pollutions occur due to more factories such as textiles, printing, rubber and etc [1]. To find a solution to this problem, the use of photocatalytic and adsorption process have recently are used [2, 3]. They are, semiconductor metal oxide have drawn much have been focus to the organic dye using UV or sunlight irradiation. The semiconductor materials in particular CuO [4], ZnS [5, 6], TiO_2 [7], ZnO [8], Fe_2O_3 [9], WO_3 [10], V_2O_5 [11], SnO_2 [12] etc., have suffered used as a photocatalyst for the removal of organic contamination. Among these, SnO_2 is the most promising n-type semiconductor with a wide band gap (3.6 eV), and its particular properties is magnetic, optical, electrical, and photocatalytic [13, 14]. Nowadays, research has been focused on the development of photocatalytic activities of SnO_2. It improves the photocatalytic efficiency of SnO_2, with metal [15] and non-metal [16]. They are, metal ions doped such as Mn, Zn, Ni, and Cu is also able to behave as an electron trapping which improves the SnO_2 photocatalytic activity due to the reducing of the e^-/h^+ recombination rate [17–21]. Finally, improved the photocatalytic efficiency of Co^{2+} doping SnO_2 are also various researchers are reported. Toloman et al., [22] have reported that the photocatalytic activity of SnO_2 was enhanced due to cobalt doping and they observed the fast trapping of photogenerated electrons by the Co dopants. Chandran et al., [23] synthesized SnO_2 with different concentration of Co^{2+} they observed a highest photodegradation of Co/SnO_2. Moreover, Mani et al., [24] prepared SnO_2 shows the band gap energy is reduced with the co-doping and they observed a highest photodegradation. Among these, non-metal is activated carbon (AC) is chosen. So, AC is a high surface area and large adsorption capacity [25]. They are SnO_2 loaded AC is supported. Furthermore, SnO_2/AC has been improved the adsorption and photocatalysts in the removal of organic dye [26]. In this work, pure SnO2, CS1, CS2, CS3 and CS2/CCAC was produced and then, the photocatalytic activity of the CS2/CCAC was evaluated via the degradation of MB under the sunlight irradiation.

2. Experiment

2.1. Synthesis of Co doped SnO_2/CCAC

Co: SnO_2/CCAC [16] was prepared as follows, firstly, $SnCl_2$ H_2O (0.5 M) was added to 50 mL and stirred for 10 min. Secondly, (0.050 M) CH_3 $COO)_2$ Co $(NO_3)_2$ $6H_2O$ solution in 20 mL of DI was added to the mixture and solution was stirred for 30 min. Thirdly, (0.75 M) $C_2H_2O_4$ $2H_2O$ solution in 50 mL of DI was added drop wise under stirring for 60 min. Similarly, in the preparation, Co: SnO_2/CCAC, a 0.5 g of CCAC was added to an above solution was stirred for 4 h. The prepared solution was filtered, ethanol washed, and then dried at 110 °C for 2 h. The dried sample was then heated at 400 °C for 2 h to form the Co: SnO_2/CCAC. The same preparation technique was implemented for all concentrations of cobalt (0.075, and 0.1 M) and pure SnO_2. The products materials were indexed as pure SnO_2, CS1, CS2, CS3, and CS2/CCAC, respectively.

2.4. Characterization

The XRD patterns of the samples were recorded by X'PERT-PRO diffractometer with a Cu Kα (1.5406 Å) radiation. The binding-state of the CS2/CCAC were characterized with X-ray photoelectron spectroscopy (XPS) (HP 5950A, Hewlett-Packard firm using monochromatic $AlK_{\alpha 1,2}$). The photoluminescence (PL) emission spectra were indexed (Jobin Yvon, FLUOROLOG-FL3-11). The surface morphologies of the pure SnO_2, CS2 and CS2/CCAC were analyzed by FE-SEM (CARL ZEISS) with Energy-dispersive X-ray spectroscopy (Bruker). An electrochemical workstation (CHI 660C) was used for measuring EIS at an open circuit potential with (0.5 M Na_2SO_4) as the electrolyte solution. The pure SnO_2, CS2 and CS2/CCAC, Ag/AgCl and pt-wire were used as the working, reference, and counter electrodes, respectively.

2.5. Photocatalytic experiment

The photocatalytic degradation of MB using pure SnO_2, CS2 and CS2/CCAC was carried out. In the photocatalytic test, 0.20 g/L catalyst under stirring was added 100 mL of MB dye solution (60 mg/L) by under adsorption dark process for 1 h. Moreover, sunlight irradiation time (solar intensity 1250 x 100 Lu ± 100) and keeping dye solutions was immediately centrifuge to remove catalyst particles. After centrifuging for every 15 min, the absorption of the MB and the supernatant solution was measured by absorption spectrophotometer (UV-1800). Then, the photodegradation of the MB was calculated as [27].

3. Results And Discussion

3.1. XRD analysis

The XRD patterns of synthesized samples are shown in Fig. 1. It was clearly seen that all the diffraction peaks can be ascribed to the rutile tetragonal structure of pure SnO_2 phase (JCPDS No. 88–0287) [28, 29]. Further no traces of other phases were observed throughout the whole range of cobalt and CCAC contents considered. However, a peak at 2 theta approximately 26.51° (110) in the XRD pattern of CS2/CCAC, indicates all the intensity reduced peaks show that the decrease upon loading CCAC. XRD

pattern (Fig. 1b) for 2 theta range is 25–35°, it can be seen that (110) and (101) in the peaks at approximately 26.51° and 33.71° has slightly shifted all the doping and loading than the pure SnO_2. Here, the ionic radius of Co^{2+} (0.58 Å) is smaller than that of Sn^{4+} (0.71 Å) and with the smaller amount of Co concentration used for doping [30]. Moreover, CS2/CCAC shows all the diffraction peaks indicate reduced compared to the other samples. The crystalline sizes of the pure SnO_2, CS1, CS2, CS3, and CS2/CCAC were calculated by using Scherrer's equation [31]. The average crystalline size of pure SnO_2, CS1, CS2, CS3, and CS2/CCAC is found to be 26.40, 24.80, 22.03, 23.41 and 18.76 nm respectively. This result suggests that the size growth is reduced due to the doping of cobalt and loading of CCAC.

3.2. XPS analysis

Surface charge states of elements show in the CS2/CCAC were analyzed using the XPS technique (Fig. 2a). On the other hand, high resolution XPS spectrums for Sn 3d, Co 2p, C 1 s and O 1 s of CS2/CCAC were observed. The peak around BE (Fig. 2b) of 486.78 and 496.24 eV represented Sn $3d_{5/2}$ and Sn $3d_{3/2}$, respectively, which confirms that the Sn ions possess intrinsic/native oxidation state of + 4 [32]. The peak around BE (Fig. 2c) of 780.15 and 786.24 eV were respectively corresponding to Co $2p_{3/2}$ and $2p_{1/2}$, which may be attributed to Co^{2+} ions [33]. The C 1 s BE (Fig. 2d) peak of CS2/CCAC was deconvoluted into three peaks at 284.18, 286.45 and 288.89 eV represented C-C, C-OH and C-O/C-O-C bonds respectively [16]. The O 1 s (Fig. 2e) BE broad peaks of CS2/CCAC revealed a single symmetrical peak at 531.28 eV which corresponds to the lattice oxygen of SnO_2.

3.3. Photoluminance analysis

The PL emission spectra of pure SnO_2, CS1, CS2, CS3, and CS2/CCAC were displayed in Fig. 3. It can be observed that, pure SnO_2 exhibit the recombination emission peak at 399 nm. Moreover, the PL spectra intensity decreased for CS2/CCAC with respect to pure SnO_2. The PL spectra intensity decreased for CS2/CCAC with respect to pure SnO_2. It observed that the emission spectra exhibited a gradually decrease the UV and visible region upon cobalt doping and CCAC loading. Furthermore, cobalt doping SnO_2/CCAC process, the excited e^-/h^+ is trapped by oxygen vacancies with the addition of Co^{2+} ions. Moreover, the excited e^- can migrate from the VB to the new energy levels introduced nearer to the CB by cobalt doping, which may be due to the reduction of PL intensity. Finally, CS2/CCAC improves photocatalytic activity due to the lower e^-/h^+ recombination rate [34].

3.4. FE-SEM with EDAX analyses

The FE-SEM micrographs of the synthesized pure SnO_2, CS2 and CS2/CCAC are shown in Fig. 4a-d along with their EDAX analysis. Figure 4a shows the spherical morphology with a size range of approximately 20–40 nm. Figure 4b shows the spherically shaped and less agglomerate with a size range of approximately 15–35 nm. Figure 4c shows the CS2 loaded on CCAC, further spherically shaped and agglomerate with a size range of approximately 10–25 nm. The chemical compositions of CS2/CCAC

(Fig. 4d) are analyzed by using EDAX. The presence of elements C, O, Sn, and Co was observed in CS2/CCAC indicated that CS2 was successfully loaded onto the CCAC.

3.5. Electrochemical impedance spectroscopy

The EIS measurements on synthesized samples are shown as Nyquist plots (Fig. 5). Meanwhile, CS2/CCAC show smaller radius in the EIS Nyquist plots than other samples, and especially, the resistance value is 3.328, 2.836 and 2.156 kΩ for the pure SnO_2, CS2 and CS2/CCAC. In addition, PL intensity of CS2/CCAC at 399 nm was much lower than that of pure SnO_2, also suggesting a faster charge separation (Fig. 3). Together with the EIS measurement, it was inferred that strong interfacial interaction between CCAC and CS2 in the accelerated the electron-hole separation and then benefit enhancement of photocatalytic activities of the as-prepared CS2 and pure SnO_2.

3.6. Photodegradation of MB dye

The UV–Vis absorption spectra of the MB dye under sunlight irradiation in the presence of pure SnO_2, CS2 and CS2/CCAC are shown in Fig. 6a-c. The intensity of the absorbance decreases with the increase of irradiation time. It can be observed that the absorption peaks (664 nm) is progressively reduced as the irradiation time (0-120 min) increase, indicative of the removal of MB dye solution. As observed in figure, CS2/CCAC removal of MB more rapidly than other sample.

Figure 7 shows the effects of contact time and % degradation of MB in the efficiency of the pure SnO_2, CS2 and CS2/CCAC. The removal efficiencies of MB at 120 min were 71.92, 83.07 and 95.38 % using pure SnO_2, CS2 and CS2/CCAC respectively. Table 1 show that the CS2/CCAC has a higher degradation percentage compared to the pure SnO_2 and CS2.

The degradation rates of the pure SnO_2, CS2 and CS2/CCAC were calculated by plotting C_t/C_0 versus irradiation time is shown in Fig. 8. As compared to pure and CS2 sample, the MB was degraded about 7.69% and 23.07% under the without sunlight, and MB was promote reduced under the photocatalytic process. Similarly, then Co^{2+} doped and CCAC loaded, their MB removal efficiency reached 43.11% and 95.38% under the dark adsorption process and photocatalytic process. Finally, the adsorption of CS2/CCAC was improved from CS2, due to the CCAC loading. Herein, the highest degradation rate in the CS2/CCAC could be the creation of huge trapping sites and generation and consequent separation of e^-/h^+ pairs. The result is explained in PL and EIS study.

The photocatalytic performance of the pure SnO_2, CS2 and CS2/CCAC was calculated by using pseudo-first-order kinetics [35, 36]. Figure 9 shows that the plot of ln (C_o/C_t) with respect to irradiation time (min) such that by linear fit of the graph, the slope of the fitted line gives the value of the rate constant (k). They are, k value and the R^2 was calculated are given in Table 1. As shown in the table, cobalt doping and CCAC loading have a higher degradation rate (0.023 min^{-1}) compared to the pure and doping sample due to the lower crystalline size, lower resistance value, and lower recombination of charge carriers.

The photocatalytic mechanisms of CS2/CCAC are shown in Fig. 10. Firstly, the increase in the photocatalytic performance of the CS2/CCAC compared to SnO_2 is due to the effect of the Co^{2+} doping and surface adsorption of the CCAC, but it also prevented the e^-/h^+ recombination. Secondly, CS2/CCAC under sunlight irradiation, the photogenerated e^- can be transferred either to the CB of SnO_2 or to Co^{2+} energy levels localized within the band gap of pure SnO_2. Co^{2+} can trap e^-/h^+ pairs as a result they can increase the e^-/h^+ lifetime [22]. Another one, e^- in CB can react with surface adsorbed O_2 to produce $^{\bullet}O_2^-$ (Eqs. 2). Moreover, h + in VB can react with the surface adsorbed H_2O/ OH^- to produce $^{\bullet}OH$ as well as attack and oxidize the MB (Eqs. 3,4). This mechanism can be described by the following equations.

$$Co:SnO_2/CCAC + h\upsilon \rightarrow e^- + h^+ \quad (1)$$

$$e^- + O_2 \rightarrow {}^{\bullet}O_2^- \quad (2)$$

$$h^+ + H_2O \rightarrow H^+ + OH^{\bullet} \quad (3)$$

$$h^+ + OH^- \rightarrow OH^{\bullet} \quad (4)$$

$$BG + OH^{\bullet} \rightarrow \text{degradation product} \quad (5)$$

$$BG + {}^{\bullet}O_2^- \rightarrow \text{degradation product} \quad (6)$$

Fig. 11 showed the reusability of CS2/CCAC (0.20 g/L) for the photodegradation of MB. The degradation rate of MB keep stable in the first and second, then slightly decreased after 3 cycles. At fourth cycles, the degradation rate of MB decreased at 93.57 %, respectively, due to the loss of photocatalytic activity of the CS2/CCAC. They are, recovered catalyst after each cycle was washed with water and ethanol, and then dried at 100 °C for 1 h and reused for next cycle. Finally, the finding supported that we can re-used CS2/CCAC for several times to reduce the treatment cost of MB.

4. Conclusion

In this study, CS2/CCAC was prepared and exhibited excellent photocatalytic degradation of MB under sunlight. The average crystalline sizes of the sample reduced (18.76 nm) with the doping and loading. Reduction of the emission peak (399 nm) with Co doping and CCAC loading into SnO_2 was observed in PL studies and its smaller value (2.156 kΩ) of impedance from EIS measurements revealing the faster transport and enhances separation of the charge carriers. They are CS2/CCAC showed a high removal efficiency of 95.38% compared to other samples. Moreover, Co^{2+} doping, CCAC not only improved the adsorption capacity, but it also prevented the e^-/h^+ recombination. Thus, CS2/CCAC may be an efficient material for removal of the MB dye solution.

References

1. S. Suarez, M. Carballa, F. Omil, J. Lema, How are pharmaceutical and personal care products (PPCPs) removed from urban wastewaters? Rev. Environ. Sci. Biotechnol. **7**(2), 125–138 (2008)
2. S.P. Kim, M.Y. Choi, H.C. Choi, Photocatalytic activity of SnO_2 nanoparticles in methylene blue degradation. Mater. Res. Bull **74**, 85–89 (2016)
3. M. Ma, H. Ying, F. Cao, Q. Wang, N. Ai, Adsorption of congo red on mesoporous activated carbon prepared by CO_2 physical activation. Chin. J. Chem. Eng. **28**, 1069–1076 (2020)
4. D. Lu, O.A. Zelekew, A.K. Abay, Q. Huang, X. Chen, Y. Zheng, Synthesis and photocatalytic activities of a CuO/TiO_2 composite catalyst using aquatic plants with accumulated copper as a template. RSC Adv. **9**, 2018–2025 (2019)
5. Z. Ye, L. Kong, F. Chen, Z. Chen, Y. Lin, C. Liu, A comparative study of photocatalytic activity of ZnS photocatalyst for degradation of various dyes. Optik **164**, 345–354 (2018)
6. J. Gajendiran, S. Gnanam, V. Vijaya Kumar, K. Ramachandran. R. Ramya, S. Gokul Raj, N. Sivakumar, Structural, optical and photocatalytic properties of ZnS spherical/flake nanostructures by sugar-assisted hydrothermal process. Chem. Phys. Lett. **754**, 137639 (2020)
7. Y. Nam, J.H. Lim, K.C. Ko, J.Y. Lee, Photocatalytic activity of TiO_2 nanoparticles: a theoretical aspect. J. Mater. Chem. A **7**, 13833–13859 (2019)
8. R. Nithya, S. Ragupathy, D. Sakthi, V. Arun, N. Kannadasan, A study on Mn doped ZnO loaded on CSAC for the photocatalytic degradation of brilliant green dye. Chem. Phys. Lett. **755**, 137769 (2020)
9. S.K. Maji, N. Mukherjee, A. Mondal, B. Adhikary, Synthesis, characterization and photocatalytic activity of α-Fe_2O_3 nanoparticles. Polyhedron **33**, 145–149 (2012)
10. X. Liu, H. Zhai, P. Wang, Q. Zhang, Z. Wang, Y. Liu, Y. Dai, B. Huang, X. Qin, X. Zhang, Synthesis of a WO_3 photocatalyst with high photocatalytic activity and stability using synergetic internal Fe^{3+} doping and superficial Pt loading for ethylene degradation under visible-light irradiation. Catal. Sci. Technol. **9**, 652–658 (2019)
11. J. Liu, R. Yang, S. Li, Synthesis and photocatalytic activity of TiO_2/V_2O_5 composite catalyst doped with rare earth ions. J. Rare Earth **25**, 173–178 (2007)
12. S. Ragupathy, T. Sathya, Synthesis and characterization of SnO_2 loaded on groundnut shell activated carbon and photocatalytic activity on MB dye under sunlight radiation. J. Mater. Sci. Mater. Electron. **27**, 5770–5778 (2016)
13. R. Zulfiqar, Y. Khan, Z. Yuan, J. Iqbal, W. Yang, Z. Wang, J. Ye, Lu, Variation of structural, optical, dielectric and magnetic properties of SnO_2 nanoparticles. J. Mater. Sci.: Mater. Electron. **28**, 4625–4636 (2017)
14. A. Ali Baig, V. Rathinam, V. Ramya, Facile fabrication of Zn-doped SnO_2 nanoparticles for enhanced photocatalytic dye degradation performance under visible light exposure. Adv Compos Hybrid Mater (2021). https://doi.org/10.1007/s42114-020-00195-9
15. F. Zahmatkeshani, M. Tohidim, Synthesis of SnO_2, Zn-doped SnO_2 and Zn_2SnO_4 nanostructure-based hierarchical architectures by using deep eutectic precursors and their photocatalytic

application. Cryst. Eng. Comm. **21**, 6758–6771 (2019)

16. M. Ramamoorthy, S. Ragupathy, D. Sakthi, V. Arun, N. Kannadasan, Synthesis of SnO_2 loaded on corn cob activated carbon for enhancing the photodegradation of methylene blue under sunlight irradiation. J. Environ. Chem. Eng. **8**, 104331 (2020)
17. L. Sakwises, P. Pisitsak, H. Manuspiya, S. Ummartyotin, Effect of Mn-substituted SnO_2 particle toward photocatalytic degradation of methylene blue dye. Results Phys **7**, 1751–1759 (2017)
18. B. Babu, A.N. Kadam, G. Thirumala Rao, S.W. Lee, C. Byon, J. Shim, Enhancement of visible-light-driven photoresponse of Mn-doped SnO_2 quantum dots obtained by rapid and energy efficient synthesis. J. Lumin. **195**, 283–289 (2018)
19. Hydrothermal synthesis of, surfactant assisted Zn doped SnO_2 nanoparticles with enhanced photocatalytic performance and energy storage performance. J. Phys. Chem. Solids **141**, 109407 (2020)
20. D. Chen, S. Huang, R. Huang, Q. Zhang, T.-T. Le, E. Cheng, Z. Hu, Z. Chen, Convenient fabrication of Ni-doped SnO_2 quantum dots with improved photodegradation performance for Rhodamine B. J. Alloys Compd. **788**, 929–935 (2019)
21. B. Babu, A.N. Kadam, R.V.S.S.N. Ravikumar, C. Byon, Enhanced visible light photocatalytic activity of Cu-doped SnO_2 quantum dots by solution combustion synthesis. J. Alloys Compd. **703**, 330–336 (2017)
22. D. Toloman, A. Popa, M. Stefan, T.D. Silipas, R.C. Suciu, L. Barbu-Tudoran, O. Pana, Enhanced photocatalytic activity of Co doped SnO_2 nanoparticles by controlling the oxygen vacancy states. Opt. Mater. **110**, 110472 (2020)
23. D. Chandran, S. Lakshmi, S. Nair, K. Balachandran, M. Rajendra Babu, Deepa, Structural, optical, photocatalytic, and antimicrobial activities of cobalt-doped tin oxide nanoparticles. J. Sol-Gel. Sci. Technol. **76**, 582–591 (2015)
24. R. Mani, K. Vivekanandan, K. Vallalperuman, Synthesis of pure and cobalt (Co) doped SnO_2 nanoparticles and its structural, optical and photocatalytic properties. J. Mater. Sci.: Mater. Electron. **28**, 4396–4402 (2017)
25. J. Saleem, U.B. Shahid, M. Hijab, H. Mackey, G. McKay, Production and applications of activated carbons as adsorbents from olive stones. Biomass Conv. Bioref. **9**, 775–802 (2019)
26. S. Begum, M. Ahmaruzzaman, Biogenic synthesis of SnO_2/activated carbon nanocomposite and its application as photocatalyst in the degradation of naproxen. Appl. Surf. Sci. **449**, 780–789 (2018)
27. A.Q. Alorabi, M. Shamshi Hassan, M. Azizi, Fe_3O_4-CuO-activated carbon composite as an efficient adsorbent for bromophenol blue dye removal from aqueous solutions. Arab. J. Chem. **13**, 8080–8091 (2020)
28. L. Aswaghosh, D. Manoharan, N. Victor, Jaya, Defect structure and optical phonon confinement in ultrananocrystalline $Bi_xSn_{1-x}O_2$ (x = 0, 0.03, 0.05, and 0.08) synthesized by a sonochemical method. Phys. Chem. Chem. Phys. **18**, 5995–6004 (2016)

29. H. ullah, I. Khan, Z.H. Yamani, A. Qurashi, Sonochemical-driven ultrafast facile synthesis of SnO_2 nanoparticles: Growth mechanism structural electrical and hydrogen gas sensing properties. Ultrason. Sonochem. **34**, 484–490 (2017)
30. M. Parthibavarman, B. Renganathan, D. Sastikumar, Development of high sensitivity ethanol gas sensor based on Co-doped SnO_2 nanoparticles by microwave irradiation technique. Curr. Appl. Phys. **13**, 1537–1544 (2013)
31. S. Ragupathy, T. Sathya, Synthesis and characterization of ZnS loaded on Pongamia pinnata shell activated carbon and photocatalytic activity on Rhodamine B dye under sunlight irradiation. J. Mater. Sci.: Mater. Electron. **28**, 3020–3028 (2017)
32. S. Jayapandi, S. Premkumar, V. Ramakrishnan, D. Lakshmi, S. Shanavas, R. Acevedo, K. Anitha, Enhanced visible light photocatalytic performance of SnO_2 nanoparticle co-doped with (Co, Nb) for organic dye degradation. J. Mater. Sci.: Mater. Electron. **31**, 10689–10701 (2020)
33. K. Srinivas, M. Vithal, B. Sreedhar, M.M. Raja, P.V. Reddy, Structural, optical, and magnetic properties of nanocrystalline Co doped SnO_2 based diluted magnetic semiconductors. J. Phys. Chem. C **113**, 3543–3552 (2009)
34. S. Bharathkumar, M. Sakar, R. Vinod, K.S. Balakumar, Versatility of electrospinning in the fabrication of fibrous mat and mesh nanostructures of bismuth ferrite ($BiFeO_3$) and their magnetic and photocatalytic activities. Phys. Chem. Chem. Phys. **17**, 17745 (2015)
35. A. Mohammad, M.E. Khan, M.R. Karim, M.H. Cho, Synergistically effective and highly visible light responsive SnO_2-g-C_3N_4 nanostructures for improved photocatalytic and photoelectrochemical performance. Appl. Surf. Sci. **495**, 143432 (2019)
36. M.S. Abdel-Wahab, A. Jilani, I.S. Yahia, A. Attieh, Al-Ghamdi, Enhanced the photocatalytic activity of Ni-doped ZnO thin films: Morphological, optical and XPS analysis. Superlattice. Microstruct. **94**, 108–118 (2016)

Table

Table 1 Photocatalytic degradation efficiency (%), rate constant (K_1) values and regression coefficient (R^2) by different prepared samples.

Samples	PDE (%)	K_1 (min^{-1})	R^2
Pure SnO_2	71.92	0.011	0.984
CS2	83.07	0.014	0.987
CS2/CCAC	95.38	0.023	0.986

Figures

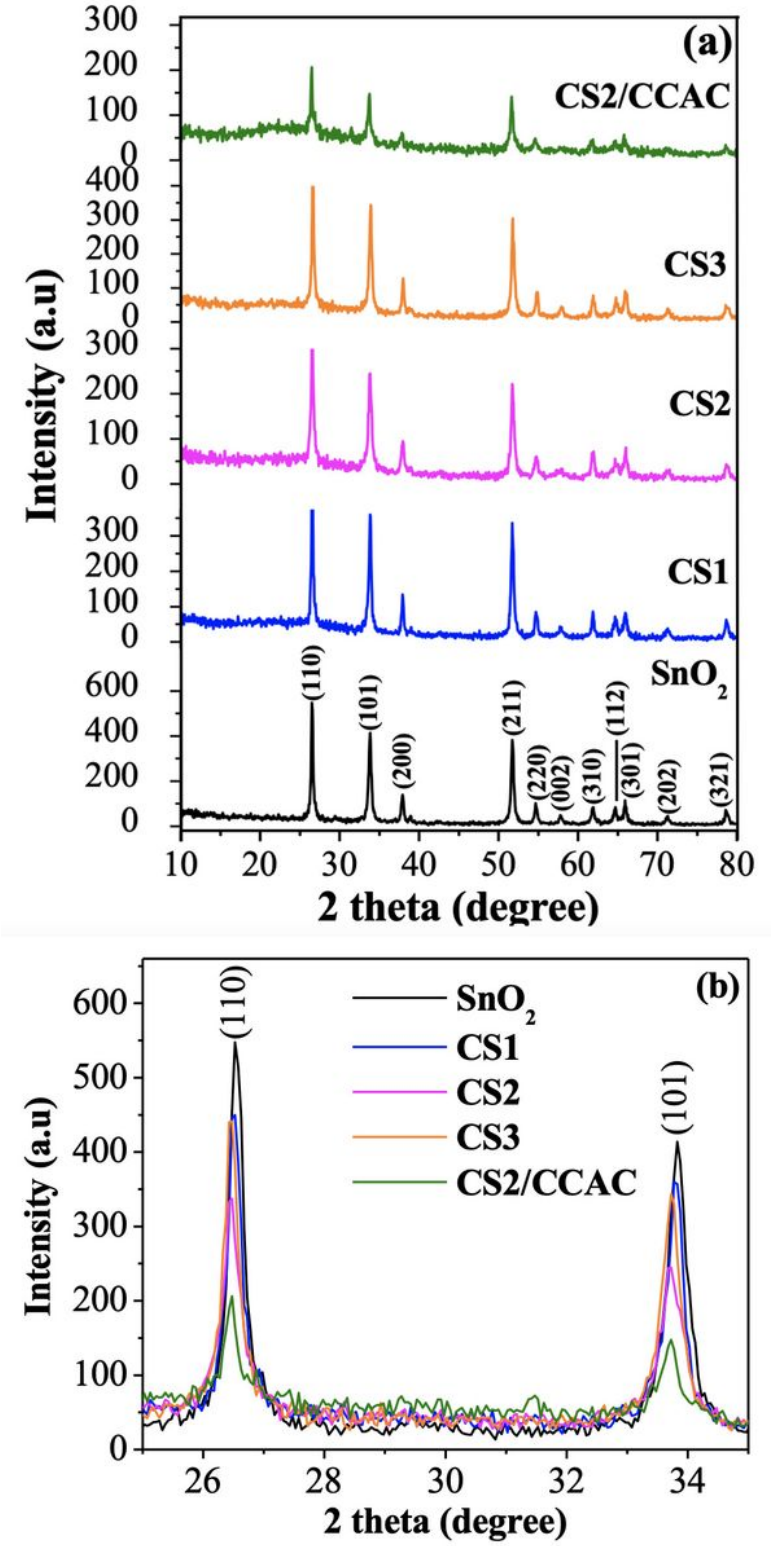

Figure 1

XRD patterns of (a) pure SnO2, CS1, CS2, CS3 and CS2/CCAC, (b) (a) pure SnO2, CS1, CS2, CS3 and CS2/CCAC enlarged view of (110) and (101).

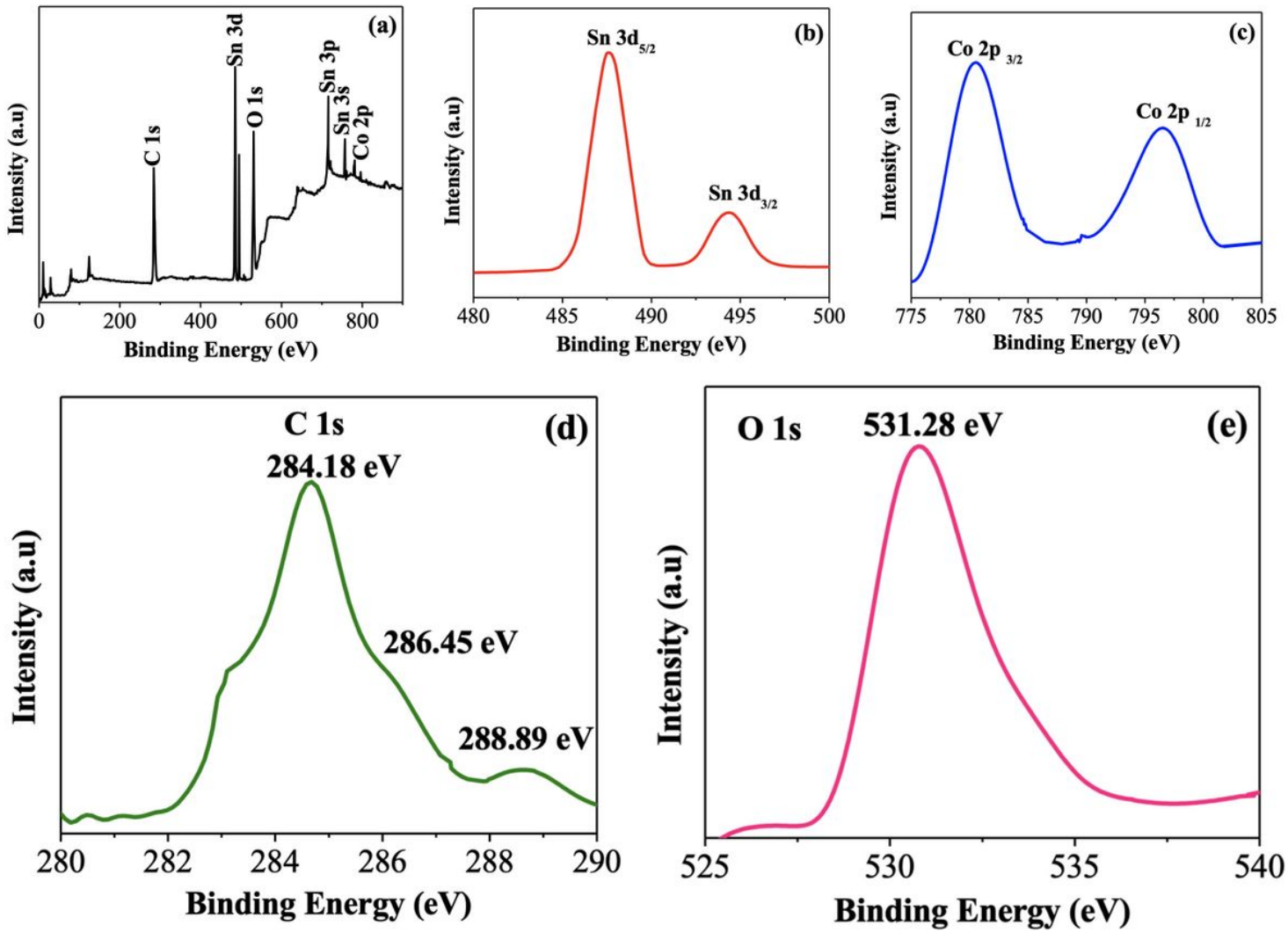

Figure 2

(a) XPS full-survey-scan spectrum, (b) Sn-3d, (c) Co-2d, (d) C1s, and (e) O1s of CS2/CCAC.

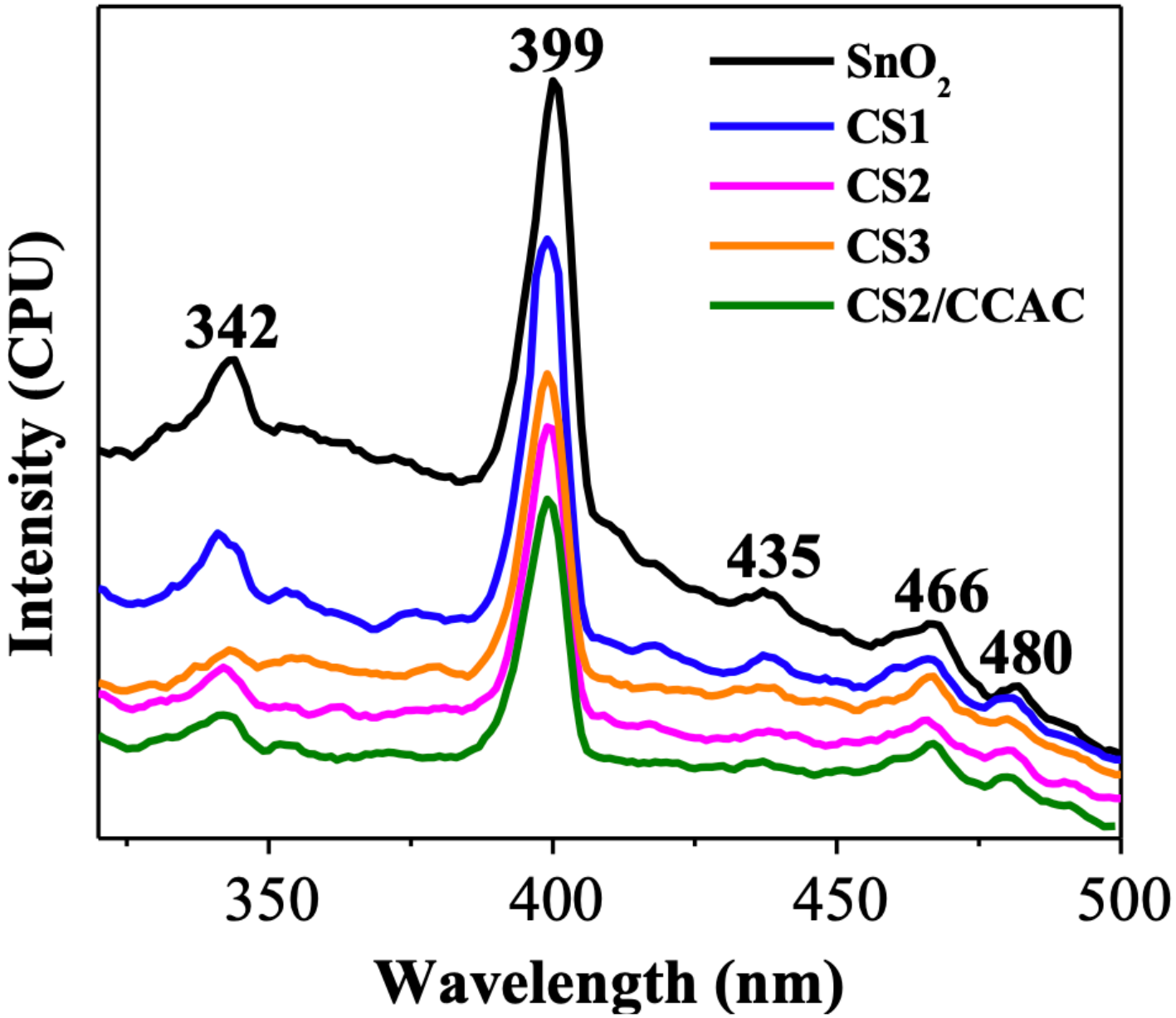

Figure 3

PL spectra of pure SnO2, CS1, CS2, CS3 and CS2/CCAC.

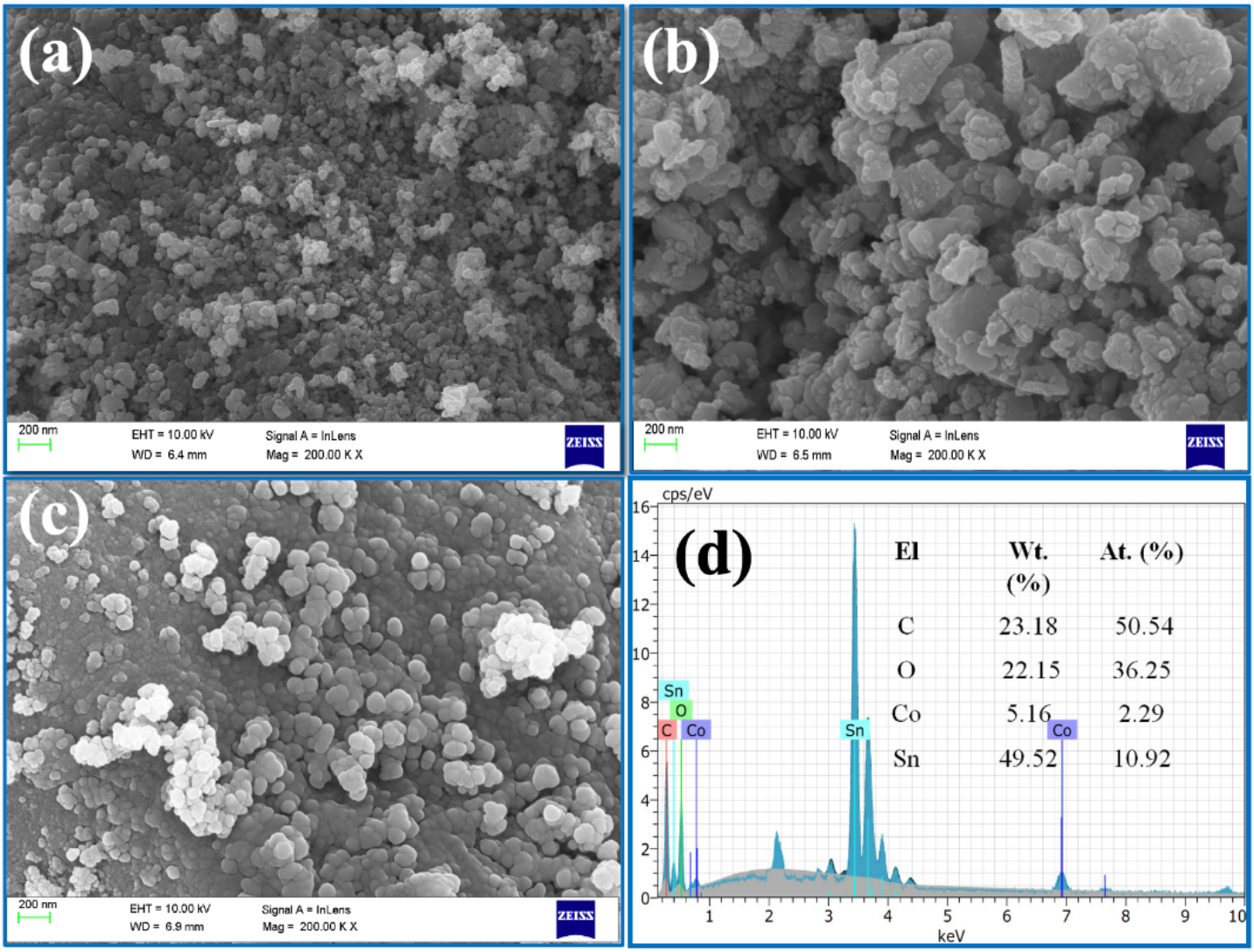

Figure 4

FE-SEM images of (a) pure SnO2, (b) CS2 and (c) CS2/CCAC, corresponding EDAX spectra (d).

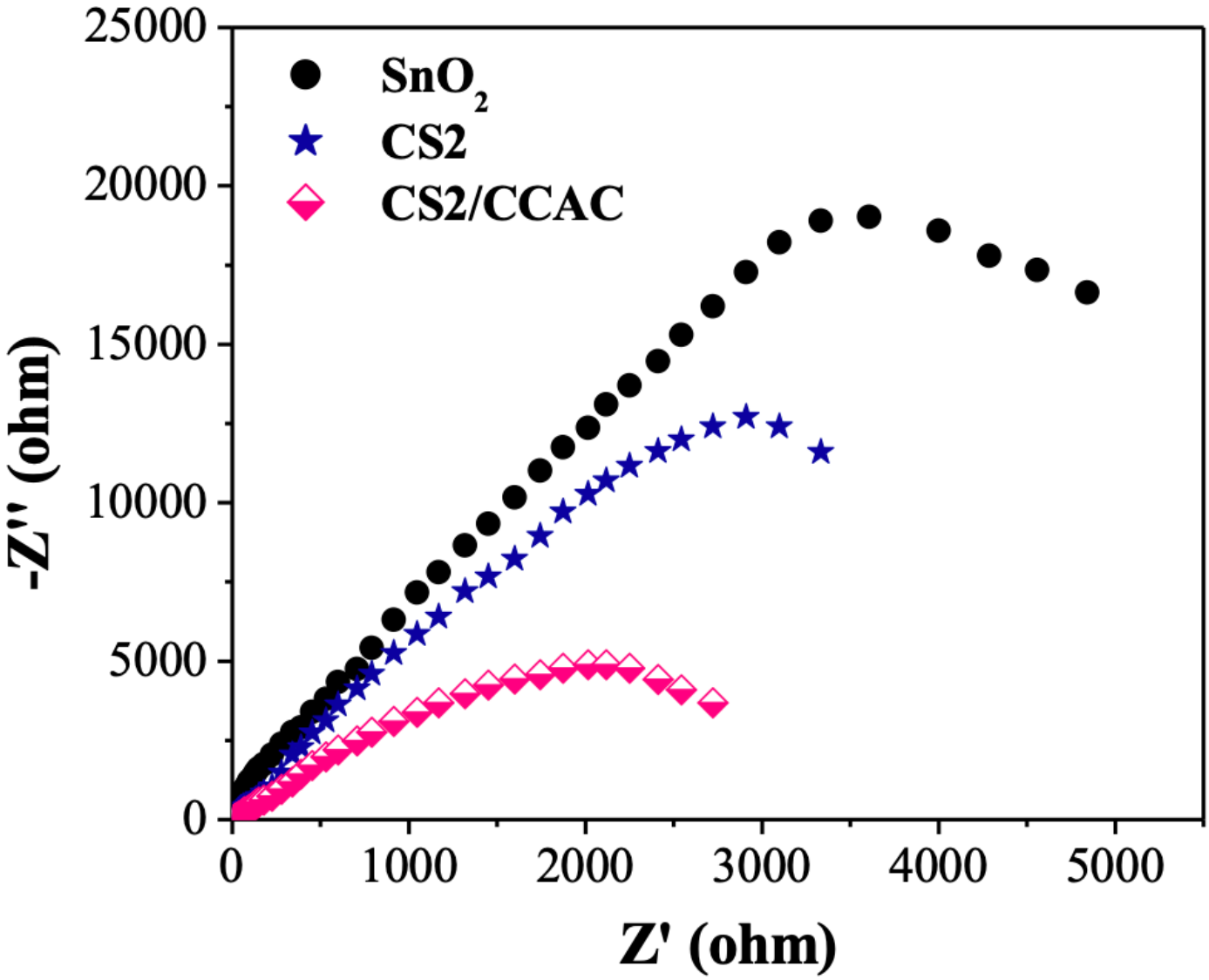

Figure 5

Nyquist plots of pure SnO2, CS2 and CS2/CCAC photocatalysts in 0.5 M Na2SO4 electrolyte.

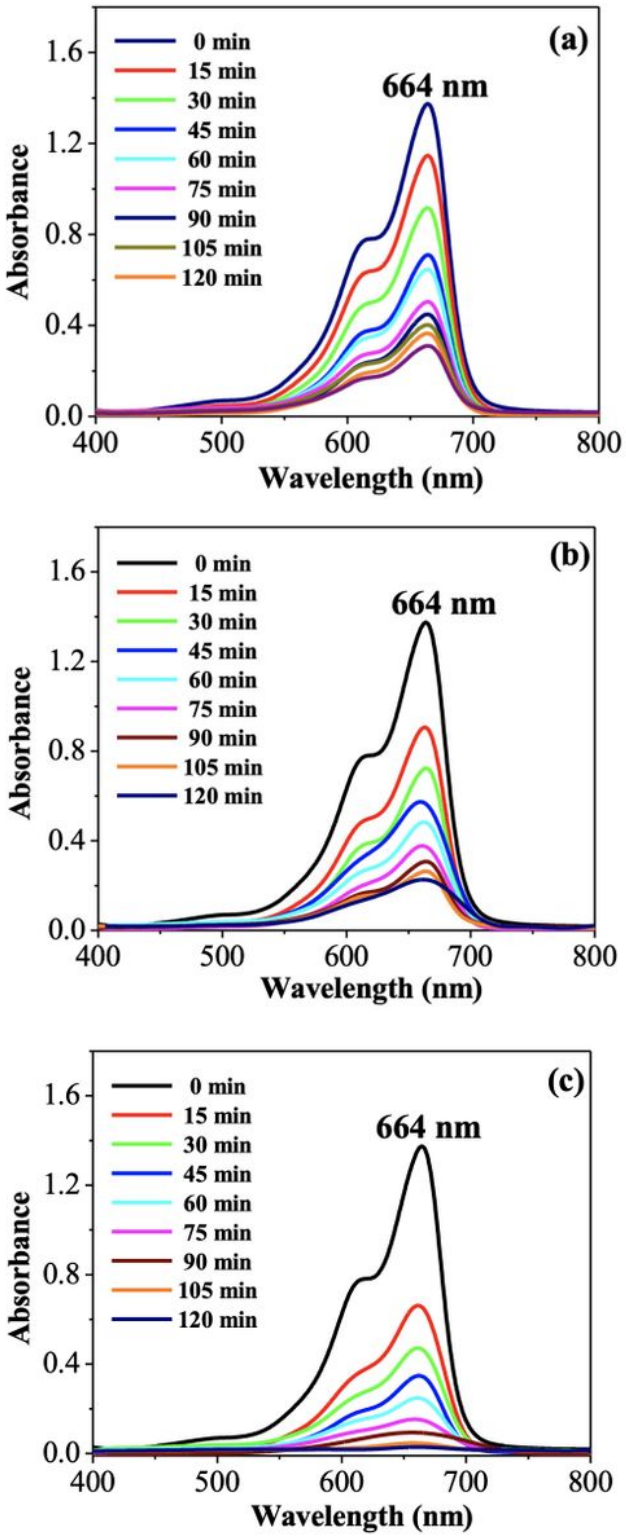

Figure 6

UV–Vis absorption spectra of the photodegradation of MB in the performance of (a) pure SnO2, (b) CS2 and (c) CS2/CCAC.

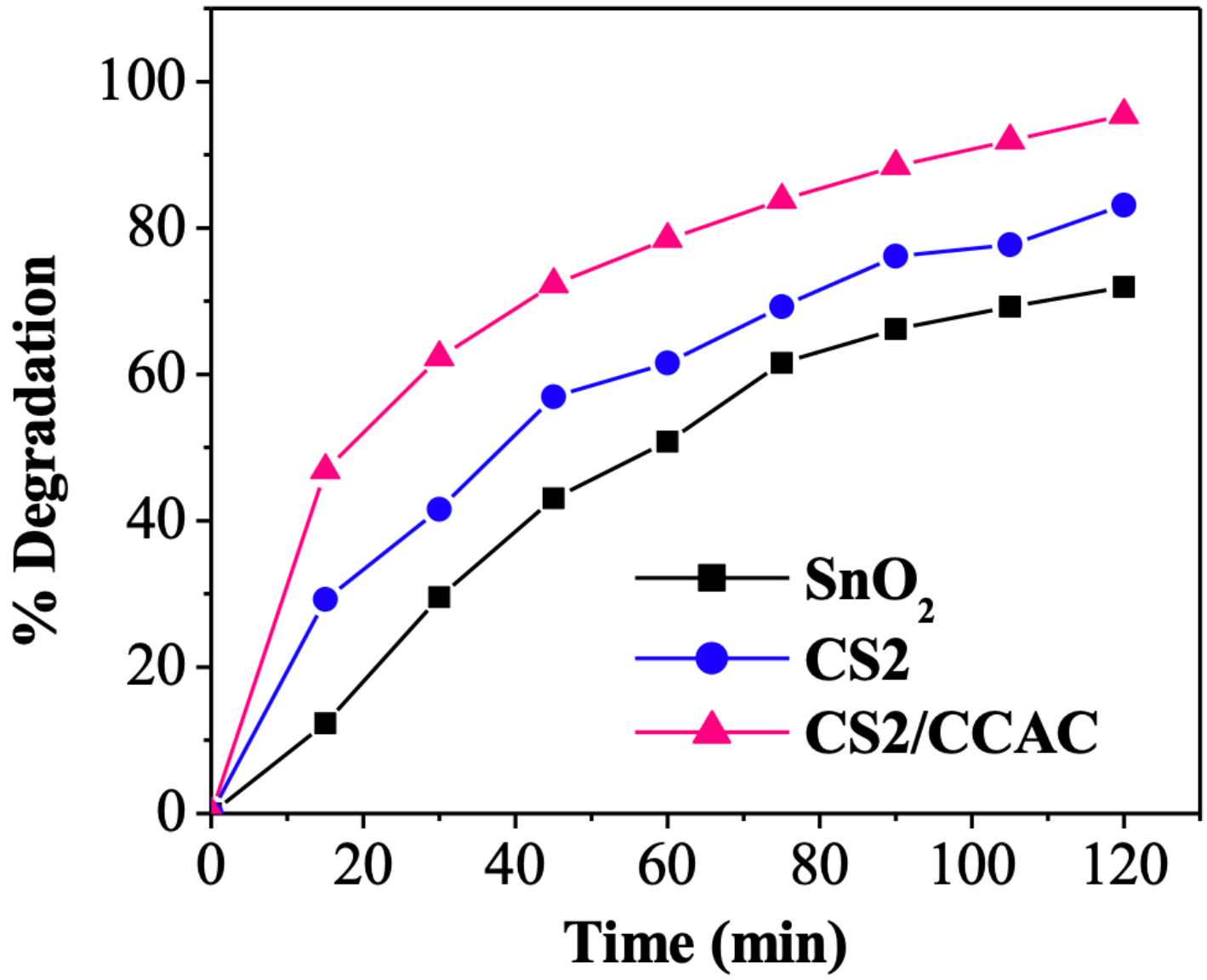

Figure 7

The effects of MB dye % degradation by pure SnO2, CS2 and CS2/CCAC.

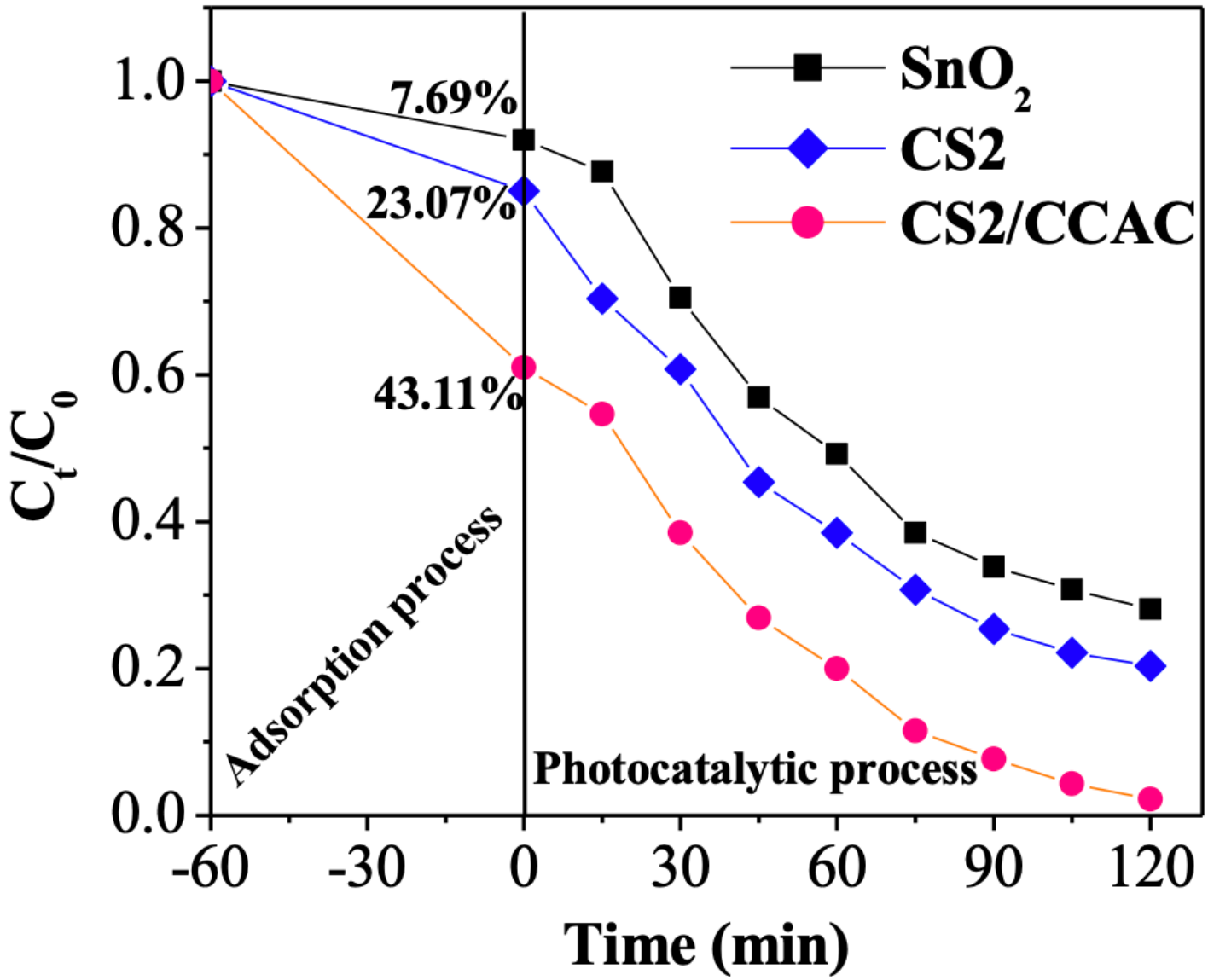

Figure 8

Photocatalytic degradation of MB dye using pure SnO2, CS2 and CS2/CCAC.

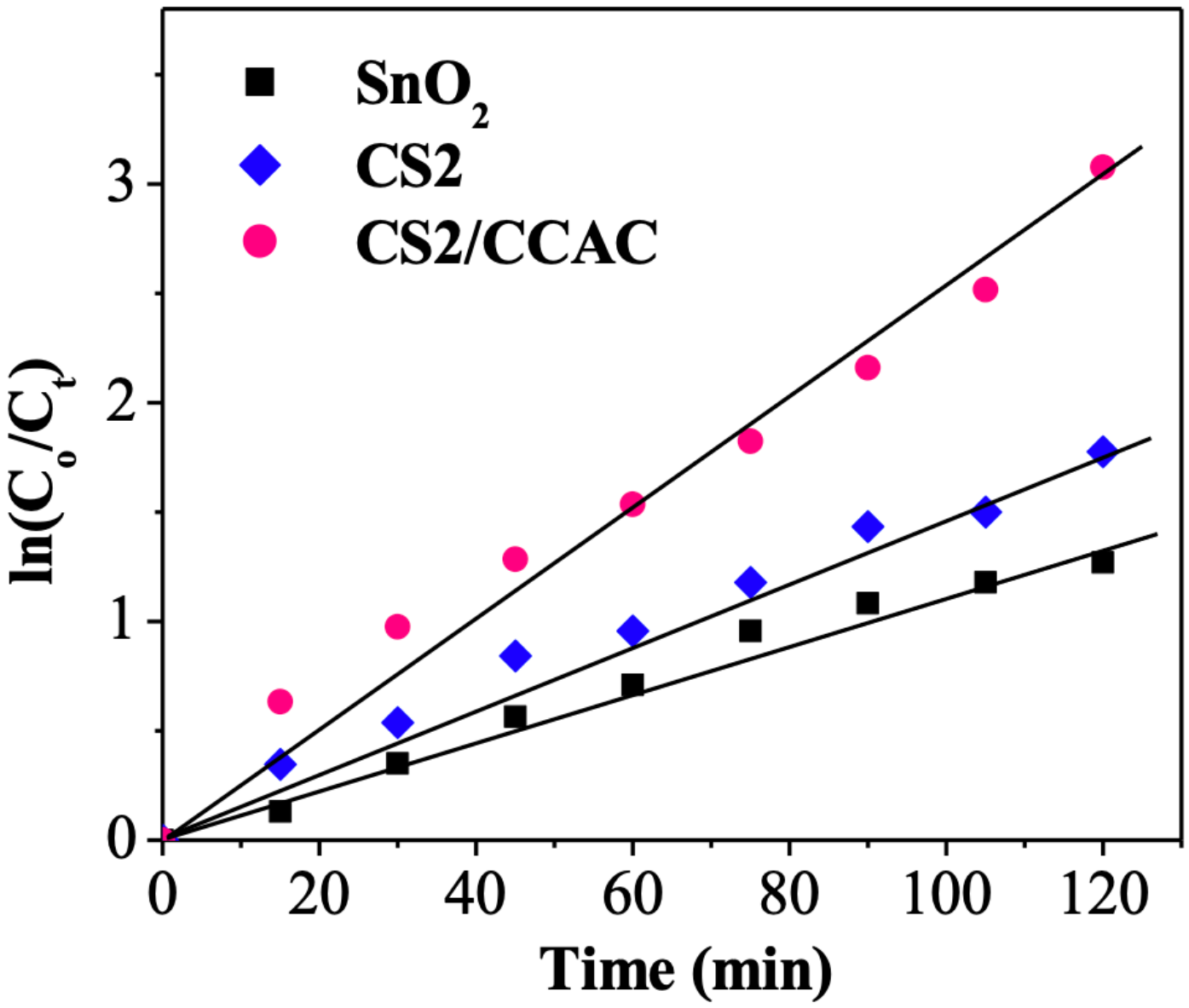

Figure 9

Kinetic study of photodegradation of MB in the presence of pure SnO2, CS2 and CS2/CCAC.

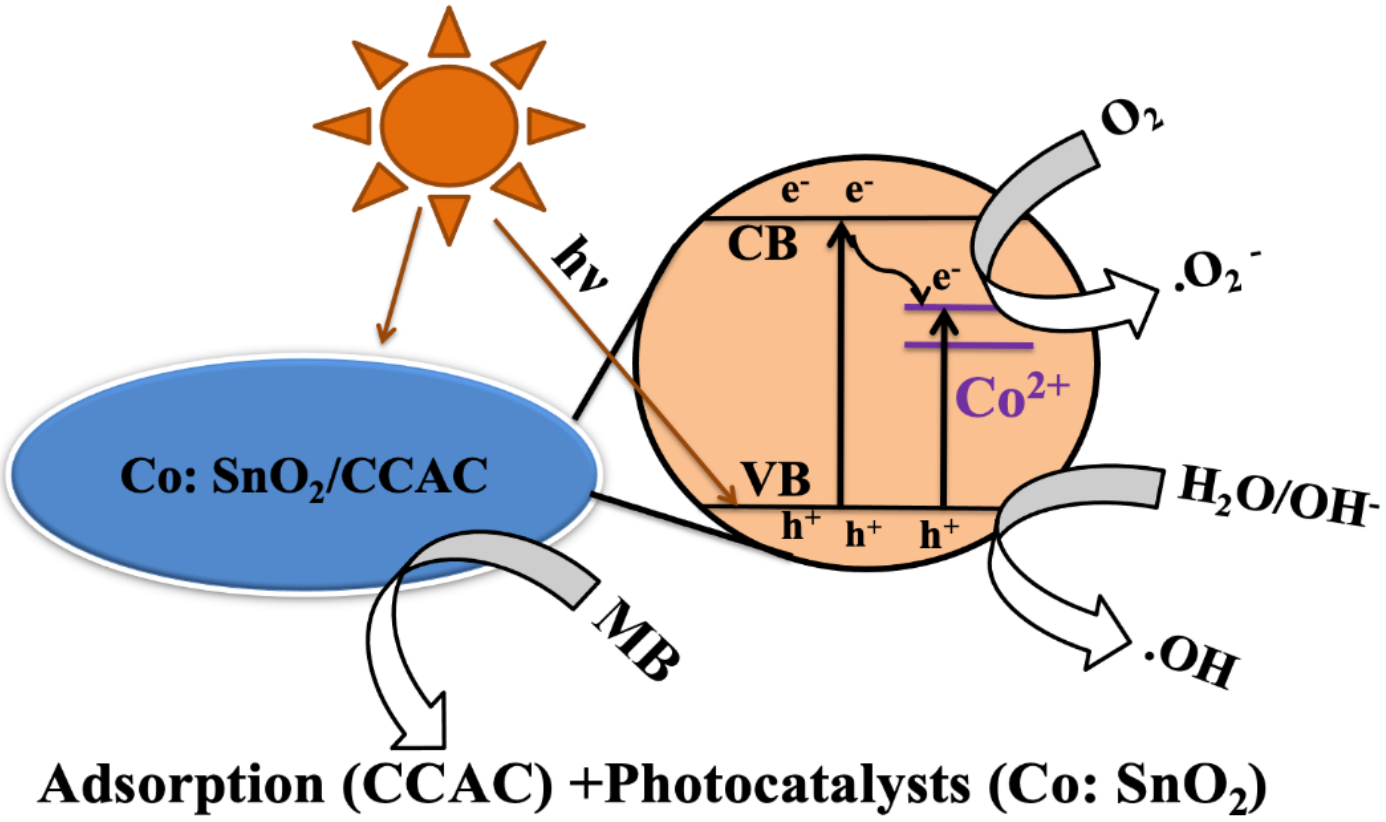

Figure 10

Schematic illustration of the photocatalytic mechanism of CS2/CCAC under sunlight irradiation.

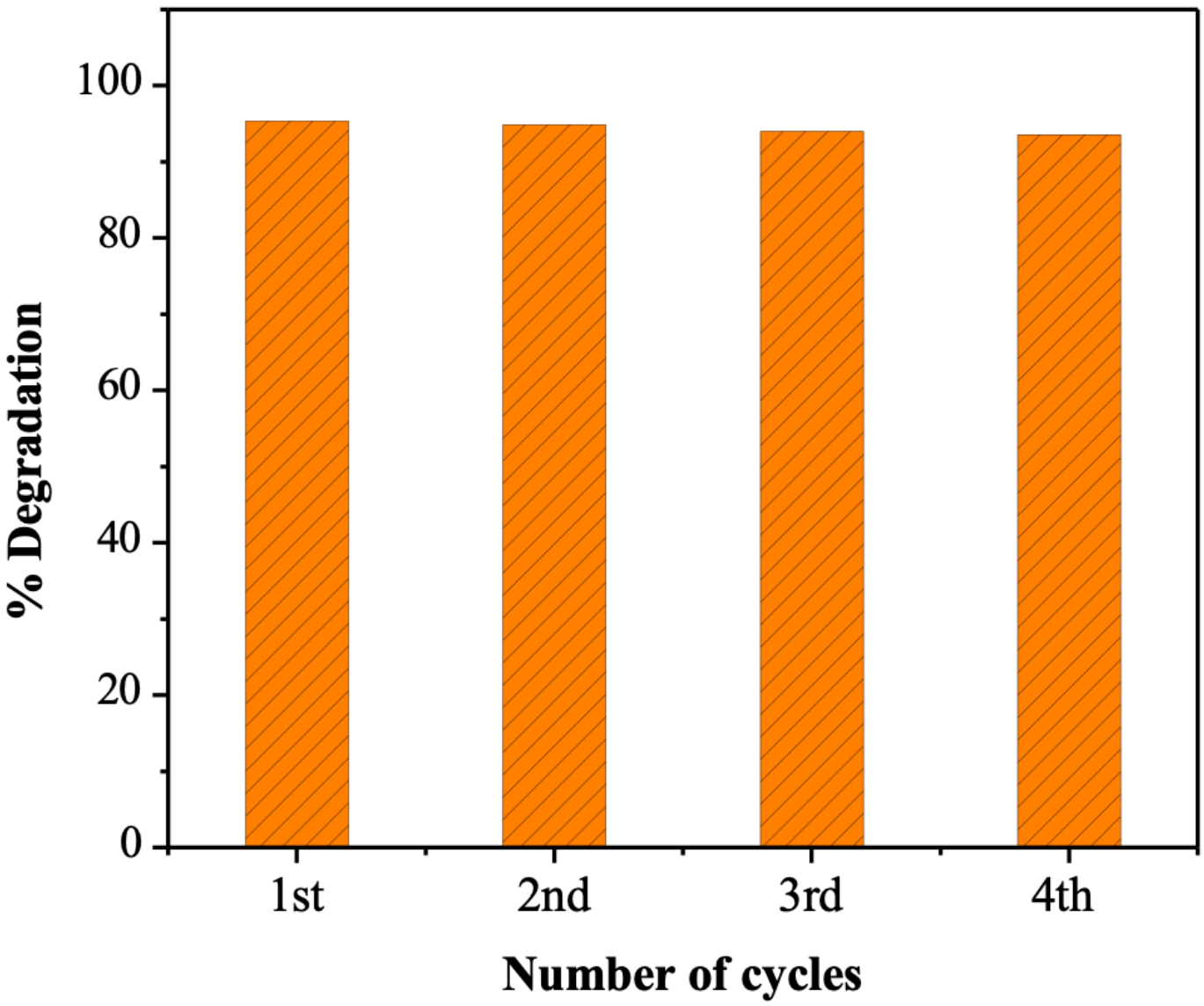

Figure 11

Recycle efficiency of the CS2/CCAC for MB degradation dye.